AIAA JOURNAL
Vol. 56, No. 3, March 2018

Utilization of Thermal Effect Induced by Plasma Generation for Aircraft Icing Mitigation

Wenwu Zhou,* Yang Liu,† and Hui Hu‡
Iowa State University, Ames, Iowa 50011
and
Haiyang Hu§ and Xuanshi Meng§
Northwestern Polytechnical University, 710072 Xi'an, People's Republic of China

DOI: 10.2514/1.J056358

An explorative investigation was performed to demonstrate the feasibility of using a thermal effect induced by dielectric-barrier-discharge plasma generation for aircraft icing mitigation. The experimental study was performed in an icing research tunnel available at Iowa State University. A NACA 0012 airfoil/wing model embedded with dielectric-barrier-discharge plasma actuators was installed in the icing research tunnel under typical glaze-/rime-icing conditions pertinent to aircraft inflight icing phenomena. While a high-speed imaging system was used to record the dynamic ice-accretion process over the airfoil surface for the test cases with and without plasma generation, an infrared thermal imaging system was used to map the corresponding temperature distributions to quantify the unsteady heat transfer and phase changing process over the airfoil surface. For the typical glaze-ice condition, the thermal effect induced by dielectric-barrier-discharge plasma generation was demonstrated to be able to prevent ice accretion over the airfoil surface during the entire ice-accretion experiment. The measured quantitative surface temperature distributions were correlated with the acquired images of the dynamic ice-accretion and water runback processes to elucidate the underlying physics.

Nomenclature

A	=	test section area; 0.4×0.4 m
C	=	chord length, 150 mm
Q	=	water flow rate
T_∞	=	incoming flow temperature
U_∞	=	airflow incoming speed
α	=	angle of attack
ρ	=	water density

I. Introduction

INFLIGHT icing is widely recognized as a significant hazard to aircraft operations in cold weather. Aircraft icing occurs when small, supercooled, airborne water droplets, which make up clouds and fog, freeze upon impacting on the airframe surface, which allows the formation of ice. Ice accretion over aircraft wings may cause the aircraft to stall at much higher speeds and lower angles of attack than normal. It will make the aircraft to roll or pitch uncontrollably, and recovery may become impossible. Petty and Floyd [1] summarized the accidents due to aircraft icing in the past 20 years, and they reported more than 800 life losses in the accidents. As described by Gent et al. [2], aircraft inflight icing can be either a rime- or glaze-icing process, depending on the flight parameters and environmental conditions. In a dry regime, all the water collected in the impingement area freezes upon impacting to form rime ice. In a wet regime, only a fraction of the collected water freezes in the impingement area to form glaze ice, and the remaining water runs back and freezes outside the impingement area. Rime ice is usually associated with colder temperatures (i.e., below −10°C), lower liquid water contents (LWC; $\rho Q/A \cdot U_\infty$), and a smaller size of the supercooled water droplets in the cloud. Glaze ice is associated with warmer temperatures (i.e., above −10°C), higher LWC levels, and larger droplet size. Because of its wet nature, glaze ice will form much more complicated shapes that are very difficult to accurately predict, and the resulting ice shapes tend to substantially deform the ice-accreting surface [3]. In general, glaze-ice formation will severely degrade the aerodynamic performance of airfoils/wings by causing large-scale flow separation, resulting in dramatic increases in drag and decreases in lift [4]. Glaze ice is also found to be harder, denser, and much more difficult to remove in comparison to rime ice. Therefore, the glaze-ice-accretion process is selected to be the primary focus of the present study.

Although a number of anti-/deicing systems have been developed for aircraft icing mitigation [5–13], current anti-/deicing strategies suffer from various drawbacks. For example, aqueous solutions of propylene and ethylene glycol (minimum of 50% concentration) along with other chemical additives are widely used for aircraft anti-/deicing at airports. Propylene and ethylene glycol, although readily biodegradable, exert an extremely high biochemical oxygen demand on aquatic systems, resulting in killing fish and other aquatic creatures due to the depletion of dissolved oxygen [14]. There have been increasing concerns about the environmental impacts from the aircraft anti-/deicing fluid swept away with storm and melt water runoff at airports to ground water and nearby waterways [15]. Although pneumatic deicing systems with rubber boots have been used to break off ice chunks accreted at the airfoil leading edge for aircraft inflight icing mitigation, they are usually heavy and sometimes unreliable [5]. Although electrothermal deicing systems have also been suggested to melt out ice by heating wing surfaces, they are usually very inefficient and require high-power input, and they may cause damage to composite materials from overheating. Furthermore, the melt water may simply run back and refreeze to cause uncontrolled ice accretion [5].

Advancing the technology for safe and efficient aircraft operation in an atmospheric icing condition requires the development of innovative, effective anti-/deicing strategies to ensure safer and more efficient operation of aircraft in cold weather. In the present study, we report the progress made in our recent efforts to explore the feasibility of using a thermal effect induced by dielectric-barrier-discharge

Received 24 May 2017; revision received 9 October 2017; accepted for publication 5 December 2017; published online 12 January 2018.

*Department of Aerospace Engineering, 2271 Howe Hall, Room 1200; also Shanghai Jiao Tong University, Gas Turbine Research Institute, School of Mechanical Engineering, 800 Dongchuan Road, 200240 Shanghai, People's Republic of China.
†Department of Aerospace Engineering, 2271 Howe Hall, Room 1200.
‡Department of Aerospace Engineering, 2271 Howe Hall, Room 1200; huhui@iastate.edu (Corresponding Author).
§Department of Fluid Mechanics, Shaanxi.

(DBD) plasma generation for aircraft icing mitigation. DBD plasma actuators, which are fully electronic devices without any moving parts, have been widely used in recent years for active flow control to suppress flow separation and airfoil stalls [16–20]. A DBD plasma actuator usually features two electrodes that are attached asymmetrically on the opposite side of a dielectric barrier sheet. When a high alternating current (ac) voltage is applied to the electrodes, the air over the encapsulated electrode will be ionized and generate a streak of plasma flow [21]. In the presence of a high-intensity electric field, the ionized air will lead to a body force that acts on the surrounding air [17]. During this process, because the ambient air over the encapsulated electrode will also be heated up by the plasma [22], the thermal effect induced by DBD plasma generation can be leveraged for anti-/deicing applications. Van den Broecke [23] was the first to conduct a feasibility study to explore the effectiveness of using DBD plasma to remove ice accretion from a stationary flat plate. More recently, Meng et al. [24] performed an experimental study to use a DBD plasma actuator to remove ice accretion over a circular cylinder. Although the feasibility of using DBD plasma for anti-/deicing applications has been demonstrated in those preliminary studies with simplified test models, the effectiveness of using DBD plasma actuators embedded over an airfoil/wing surface for aircraft icing mitigation under typical glaze-/rime-icing conditions has never been explored.

In the present study, an explorative study was performed to evaluate the effectiveness of using the thermal effect induced by DBD plasma generation for aircraft icing mitigation. The experimental study was performed in an icing research tunnel available at Iowa State University (i.e., ISU-IRT). A NACA 0012 airfoil/wing model embedded with DBD plasma actuators was installed inside the test section of the ISU-IRT under typical glaze- and rime-icing conditions pertinent to aircraft inflight icing phenomena. During the experiments, while a high-speed imaging system was used to record the dynamic ice accretion and water runback process over the surface of the airfoil/wing model, with and without switching on the DBD plasma actuators, an infrared thermal imaging system was used to map the corresponding surface temperature distributions over the airfoil surface simultaneously. The effectiveness of using the thermal effect induced by plasma generation for aircraft icing mitigation was examined in detail based on the side-by-side comparisons of the measurement results for the plasma-on case against those of the plasma-off case under the same icing conditions. The quantitative surface temperature measurement results were correlated with the acquired ice-accretion images to elucidate the underlying physics.

II. Experimental Setup and Test Model

As shown schematically in Fig. 1, the experimental study was performed in the icing research tunnel available at the Aerospace Engineering Department of Iowa State University. The icing research tunnel has a test section of 2.0 m in length by 0.4 m in width by 0.4 m in height, with four optically transparent sidewalls. The ISU-IRT has a capacity of generating a maximum wind speed of 60 m/s and an airflow temperature of −25°C. An array of pneumatic atomizer/spray nozzles are installed at the entrance of the contraction section upstream of the test section to inject microsized water droplets ($10 \sim 100$ μm in size) into the airflow. The median volume diameter of the droplets is approximately 40 μm in the present study. By manipulating the water flow rate (Q) through the water spray nozzles, the liquid water content level of the incoming airflow in the test section of the ISU-IRT can be adjusted to a desirable level, where ρ is the water density, Q is the water flow rate, A is the test section area, and U_∞ is the airflow incoming speed. In summary, the ISU-IRT can be used to simulate the aircraft inflight icing phenomena over a range of icing conditions (i.e., from dry rime- to extremely wet glaze-ice conditions). In the present study, although the freestream velocity U_∞ of the incoming airflow is kept constant at $U_\infty = 40$ m/s, the LWC level and temperature T_∞ of the incoming airflow are varied from 1.0 to 3.0 g/m^3 and from $= -5$ to $= -15$°C to simulate different (i.e., either rime or glaze) icing conditions.

The airfoil/wing model used in the present study has the profile of a NACA 0012 airfoil in the cross-section with a chord length of $C = 150$ mm and a spanwise length of $L = 400$ mm (i.e., same dimension as the width of the ISU-IRT test section). The test model, which was manufactured by using a rapid prototyping machine (i.e., three-dimensional printing) that built the model layer by layer with a resolution of about 25 μm, is made of a hard plastic material. The airfoil/wing model was finished with a coating of primer and wet sanded to a smooth finish using 1000-grit sand paper. Supported by a stainless-steel rod, the airfoil/wing model was mounted at its quarter-chord and oriented horizontally across the middle of the test section. The angle of attack α of the airfoil/wing model was set at $\alpha = -5.0$ deg during the ice-accretion experiment.

As shown schematically in Fig. 2, two sets of DBD plasma actuators were embedded over the pressure side of the airfoil surface. The DBD plasma actuators were arranged symmetrically to the middle span of the airfoil/wing model. During the experiment, while the DBD plasma actuators on the left side of the airfoil/wing model were turned on, the DBD plasma actuators over the right side would be kept off. The ice-accretion process over the airfoil surface for the plasma-on side (i.e., left side) would be compared side by side against that over the plasma-off side (i.e., right side) in order to evaluate the effectiveness of using the thermal effect induced by DBD plasma generation for aircraft icing mitigation under the identical icing conditions. For the present study, the DBD plasma actuators embedded over the airfoil surface consisted of copper electrodes with a thickness of about 70 μm. Three layers of Kapton film (130 μm for each layer) were used as the dielectric barrier to separate the encapsulated electrodes from the exposed electrodes. Ranging from the airfoil leading edge to around 30% of the airfoil chord, four encapsulated electrodes were distributed evenly along the airfoil chord with a separation distance of 3.0 mm. Although the buried electrodes had a chordwise width of 10.0 mm (except the first electrode at 5.0 mm in width), the exposed electrodes, which were placed above the dielectric barrier with zero overlaps against the covered electrodes, were 96 mm in length and 3.0 mm in width. Finally, the airfoil/wing model was finished with two layers of white

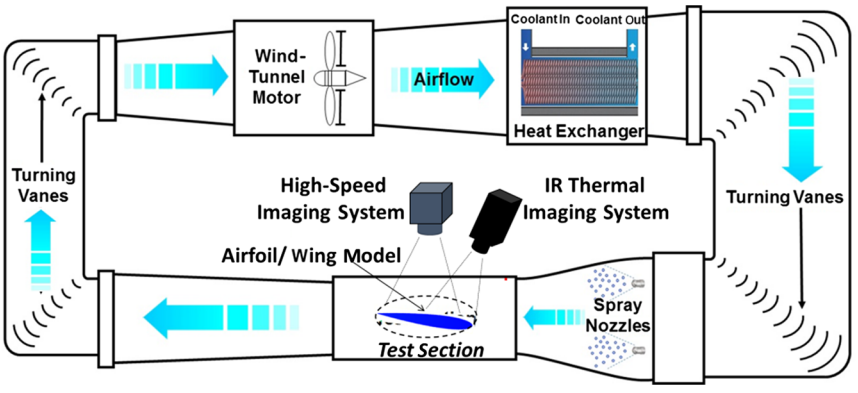

Fig. 1 Experimental setup used in the present study.

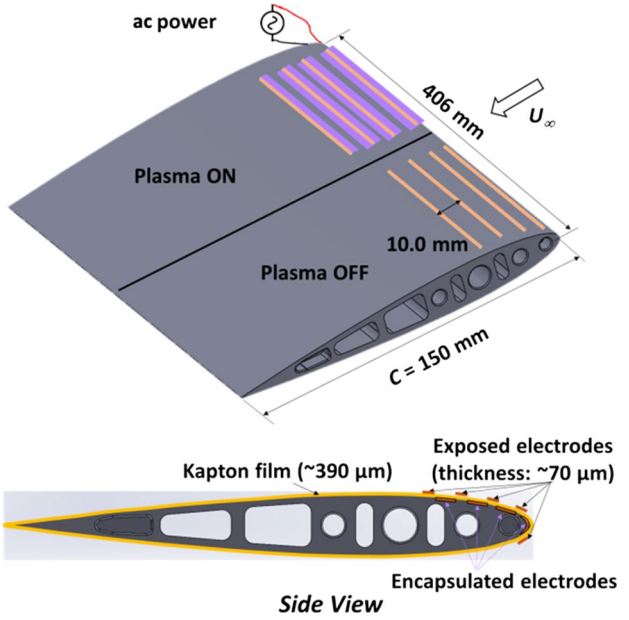

Fig. 2 Schematic of airfoil/wing model used in the present study.

enamel coating and wet sanded to a smooth surface by using 2000-grit sand paper.

During the experiments, the DBD plasma actuators on the left side of the airfoil/wing model were powered by a high-voltage alternating current power source (Nanjing Suman Company, model CTP-2000 K) with an output voltage of $V_{p-p} = 6.71$ kV (i.e., peak-to-peak value) and a constant frequency of $f = 8.9$ kHz. Although the ac current was measured by using a high-response current probe (Pearson Electronics, Inc., model Pearson 2877), the voltage was monitored by using an oscilloscope (Tektronix DPO3054). Following the work of Dong et al. [25], the power inputs P to the ac DBD plasma actuators were calculated, which were found to be $P = 102$ W for the present study. The corresponding power density ($q = P/A_p$) was found to be 25.3 kW/m^2, where A_p was the covered area of the plasma actuators (i.e., 96×42 mm).

In the present study, a high-speed imaging system (PCO Tech, Dimax, with a spatial resolution of 2000 by 2000 pixels) along with a 60 mm optical lens (Nikon, 60 mm Nikkor 2.8D) were used to record the dynamic ice-accretion process over the pressure side of the airfoil surface. As shown schematically in Fig. 1, the high-speed imaging system was mounted above the airfoil/wing model with a measurement window size of 210×210 mm (i.e., with a spatial resolution of 9.5 pixels/mm) to record the ice-accretion or water runback process over both the plasma-on and plasma-off sides of the airfoil surfaces simultaneously. An infrared (IR) thermal imaging system (FLIR-A615) was used to map the corresponding temperature distributions over the surface of the airfoil/wing model during the ice-accretion process simultaneously. The measurement uncertainty for the IR thermal imaging system was estimated to be within ±0.50°C. For acquiring the IR thermal images, an infrared emission transmissible window (FLIR IR Window-IRW-4C) was embedded on the top plate of the ISU-IRT test section. The IR thermal imaging system was focused on the front portion (i.e., the region near the airfoil leading edge) of the airfoil/wind model with a measurement window size of 110×90 mm. As a result, the spatial resolution of the IR thermal images was 5.3 pixels/mm. Before conducting the ice-accretion experiment, an in situ calibration experiment was performed to validate the IR thermal imaging system by using high-precision thermocouples in the range of 20 to −20°C. The differences between the measurement results of the IR thermal imaging system and those of the thermocouples were found to be within ±0.50°C. During the experiment, both the high-speed imaging system and the IR thermal imaging system were connected to a digital delay generator (Berkeley Nucleonics, model 575) to synchronize the timing for the image acquisitions after switching on the spray system of the ISU-IRT to start the ice-accretion process.

III. Measurement Results and Discussions

A. Effects of Plasma Generation on Ice-Accretion Under Glaze-Icing Conditions

In performing the ice-accretion experiments, the ISU-IRT was operated at a prescribed frozen temperature level (e.g., $T_\infty = -5$ and −15°C for the present study) for at least 20 min in order to ensure the ISU-IRT reaching a thermal steady state. Then, the DBD plasma actuators embedded over the left side of the airfoil/wind model were switched on for about 10 s before turning on the water spray system of the ISU-IRT. After the water spray system was switched on at $t = 0$ s, the supercooled water droplets carried by the incoming airflow would impinge onto the surface of the airfoil/wing model to start the ice-accretion process. During the experiments, the high-speed imaging system and the IR thermal imaging system were synchronized with the switch of the ISU-IRT water spray system to reveal the dynamic ice-accretion process over the airfoil surface simultaneously.

Figure 3 shows four typical snapshots of the instantaneous ice-accretion images acquired by using the high-speed imaging system under the glaze-icing condition of $U_\infty = 40$ m/s, $T_\infty = -5$°C, and LWC = 1.50 g/m^3. The box in red dashed lines in Fig. 3 indicates the measurement window of the IR thermal imaging system, and the corresponding surface temperature distributions measured simultaneously by using the IR thermal imaging system are given in Fig. 4. Note that, because very similar features were also observed for other test cases, only the measurement results obtained under the test condition of LWC = 1.5 g/m^3 were shown and analyzed here for conciseness.

As shown clearly in Fig. 3a, at the very beginning of the ice-accretion experiment (i.e., at the time instance of $t = 0.3$ s), although

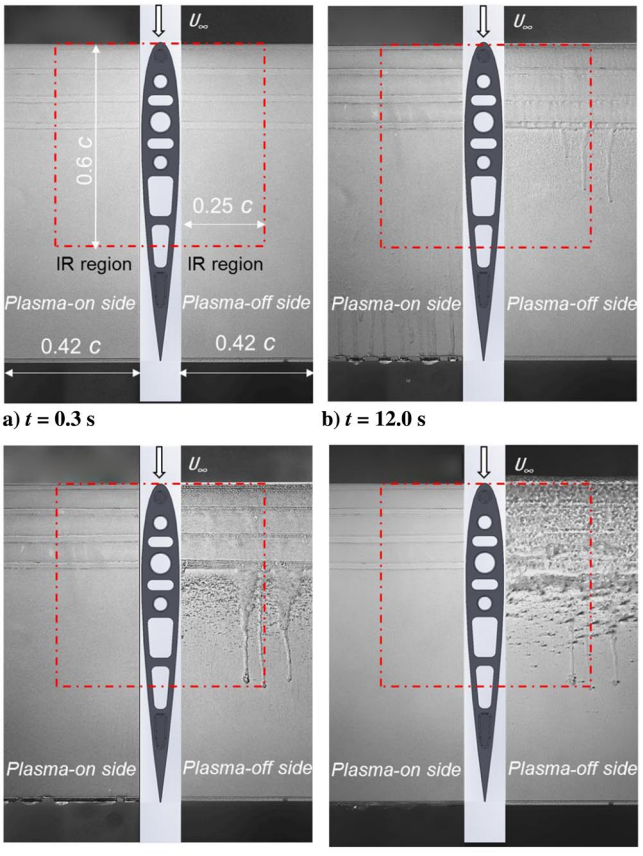

Fig. 3 Typical snapshots of the dynamic ice-accretion process over the airfoil surface under the glaze-icing conditions of $U_\infty = 40$ m/s, $T_\infty = -5$°C, and LWC = 1.50 g/m^3.

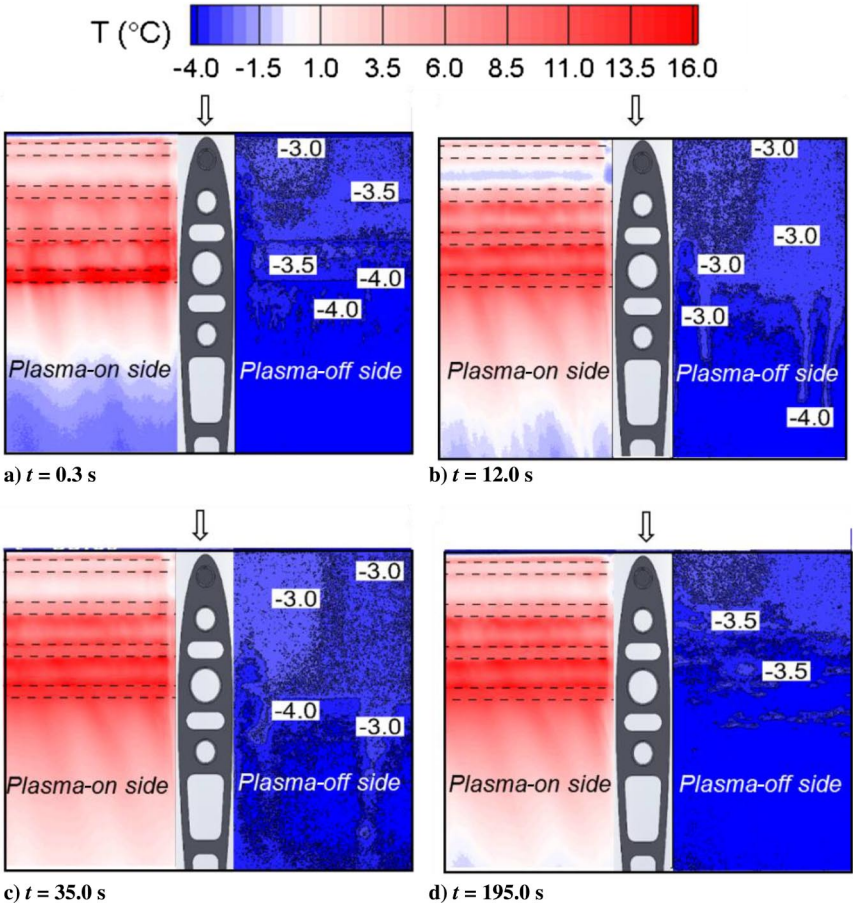

Fig. 4 Corresponding surface temperature distributions over the plasma-on and plasma-off sides of the airfoil surface under the glaze-icing conditions of $U_\infty = 40$ m/s, $T_\infty = -5$°C, and LWC = 1.50 g/m^3.

no obvious ice accretion was observed on both the plasma-on side and plasma-off sides of the airfoil surface in the snapshot image acquired by using the high-speed imaging system, the measured surface temperature distributions over the plasma-on side of the airfoil surface were found to be significantly different from those of the plasma-off side. As revealed clearly from the measured surface temperature distributions given in Fig. 4a, due to the release of the latent heat associated with the solidification process of the impinged supercooled water droplets over the airfoil surface (i.e., phase changing process from liquid state of water to solid state of ice), the surface temperatures in the region near the airfoil leading edge (i.e., the direct impinging region of the supercooled water droplets) on the plasma-off side of the airfoil surface were found to increase slightly (i.e., airfoil surface temperatures were found to increase from −5.0 up to −3.0°C), as expected. Because the surface temperatures were still found to be below the "frozen temperature" of water (i.e., $T_w < 0$°C), a thin layer of ice would be formed immediately after the supercooled water droplets impinged onto the plasma-off side of the airfoil surface. Because the ice layer formed over the airfoil surface was very thin at the time instance of $t = 0.3$ s, it was almost unobservable in the snapshot image acquired by the high-speed imaging system given in Fig. 3a.

However, as revealed clearly in the measured surface temperature distributions given in Fig. 4, due to the thermal effect induced by the DBD plasma generation as described by Joussot et al. [22], the surface temperature on the plasma-on side of the airfoil model was found to be well above the frozen temperature of water (i.e., $T_w > 0$°C). It suggests that, upon impinging onto the plasma-on side of the airfoil surface, the supercooled water droplets would be heated up. As a result, a layer of "warm" water film, instead of ice, would be formed over the airfoil surface. Thus, no ice was found to form over the plasma-on side of the airfoil surface, as shown clearly in Fig. 3.

As the ice-accretion experiment went on, more supercooled water droplets carried by the incoming airflow would impinge onto the airfoil surface. Due to the relatively warm temperature (i.e., $T_\infty = -5$°C) and high LWC level (i.e., LWC = 1.5 g/m^3) of the incoming airflow for this test case, the icing process over the airfoil surface would be of typical glaze-ice accretion if no anti-/deicing measures were applied. Similar to the scenario described by Waldman and Hu [7], with the continuous impingement of the supercooled water droplets onto the airfoil surface, more and more latent heat of fusion would be released to cause the slight temperature increase on the plasma-off side of the airfoil surface, as revealed quantitatively from the measured surface temperature distributions shown in Fig. 4. Because the heat transfer process was not fast enough to remove all of the released latent heat of fusion from the liquid water for this test case, only a portion of the impinged supercooled water droplets would be frozen into solid ice upon impacting onto the airfoil surface. The rest of the impinged water mass was found to stay in liquid state. As shown clearly at the plasma-off side of the acquired image given in Fig. 3b (i.e., the snapshot at the time instance of $t = 12.0$ s), as driven by the boundary-layer airflow above the airfoil surface, the unfrozen water film flow was found to run back and form multiple fingerlike rivulet structures in the further downstream region. It also can be seen clearly that the runback surface water on the plasma-off side was found to eventually be frozen into solid ice at the further downstream region (i.e., in the region beyond of the direct impingement area of the supercooled water droplets).

However, as shown in the snapshot image given in Fig. 3b, the left side (i.e., plasma-on side) of the airfoil surface was still found to be completely free of ice, due to the thermal effects induced by the DBD plasma generation. The surface temperature distributions given in Fig. 4 revealed quantitatively that the surface temperatures on the plasma-on side of the airfoil model were still well above the frozen temperature of water (i.e., $T_w > 0$°C). Especially in the regions where the plasma actuators were embedded, the local surface temperature was found to reach up to 15°C. As a result, instead of

being frozen into solid ice, the supercooled droplets were heated up immediately after impacting onto the plasma-on side of the airfoil surface. Similar to what was described by Zhang et al. [26], the surface water mass on the plasma-on side was found to form a thin-film flow at first in the region near the airfoil leading edge, and then run back along the airfoil surface as driven by the boundary-layer airflow over the airfoil/wing model. As shown clearly in the snapshot image given in Fig. 3b, as the water film advanced downstream, isolated water rivulets were found to form further downstream, resulting in isolated water transport channels to transport the surface water mass collected at the leading edge from the continuous impingement of the water droplets. Eventually, the impinged surface water mass was found to shed from the airfoil trailing edge.

As time went by, more and more supercooled water droplets carried by the incoming airflow would impinge onto the airfoil surface. As shown clearly in the acquired images given in Figs. 3c and 3d (i.e., the snapshots captured at the time instances of $t = 35$ s and $t = 195$ s), the ice layers accumulated on the plasma-off side of the airfoil surface were found to become thicker and thicker. The corresponding surface temperature distributions given in Figs. 4a and 4d also confirmed the existence of ice layers accreted over the plasma-off side surface by having the temperatures lower than the frozen temperature of water (i.e., $T_w < 0°C$). However, as shown quantitatively in Figs. 4c and 4d, the surface temperatures on the plasma-on side of the airfoil were still found to be well above the frozen temperature of water (i.e., $T_w > 0°C$). As a result, the plasma-on side of the airfoil surface was always found to be free of ice over the duration of the entire ice-accretion experiments (i.e., up to 300 s), as revealed clearly in Fig. 3.

In summary, the present study demonstrates clearly that, in addition to being widely used as an effective flow control method to suppress large-scale flow separation and airfoil stall, DBD plasma actuators can be used as a promising anti-/deicing tool for aircraft icing mitigation.

B. Evolution of Airfoil Surface Temperature Under Glaze-Icing Conditions

Based on the time sequences of the acquired IR thermal imaging measurement results, the evolution characteristics of the surface temperature distributions over the airfoil surface during the ice-accretion experiment can be evaluated quantitatively. As shown clearly in Fig. 4, due to the released latent heat of fusion associated with the phase changing of the impinged supercooled water droplets, the surface temperatures on the plasma-off side of the airfoil/wing model were found to change only slightly during the ice-accretion process, which was analyzed in detail in the previous study of Liu et al. [6]. The focus of the present study is on the plasma-on side of the airfoil surface to gain further insight into the underlying physics pertinent to using the thermal effects induced by plasma generation for aircraft icing mitigation.

Figure 5 shows the extracted surface temperature profiles along the chordwise direction at the centerplane of the plasma-on side of the airfoil/wing model (i.e., along the line of A-A, as shown in Fig. 5) under the test conditions of $U_\infty = 40$ m/s, $T_\infty = -5°C$, and LWC $= 1.50$ g/m^3 at the time instances of $t = 0.3$, 10, 20, 40, and 80 s, respectively. The locations of the exposed electrodes of the DBD plasma actuators were also shown in the plot for comparison. It can be seen clearly that the airfoil surface temperatures were found to vary significantly along the chordwise direction of the airfoil/wing model, featured by the irregular sawtoothlike structures in the profiles. As shown clearly in Fig. 5, the appearance of the sawtoothlike structures was found to be correlated well with the locations of the interfaces between the exposed electrodes and the embedded electrodes of the DBD plasma actuators. It indicates that the DBD plasma generation at the electrode interfaces would induce a maximum local temperature, which agrees well with the findings reported in the previous study of Joussot et al. [22].

The measurement results given in Fig. 5 also reveal clearly that, due to the thermal effect induced by the DBD plasma generation, the surface temperatures in the regions near the plasma actuators were found to be always well above the frozen temperature of water (i.e., $T_w > 0°C$),

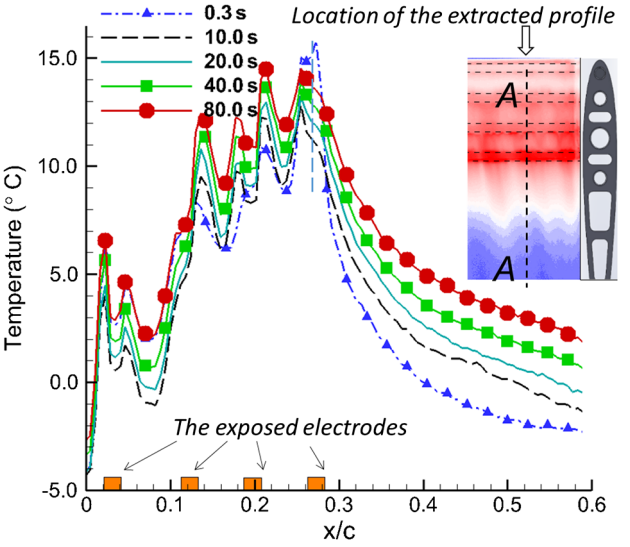

Fig. 5 Extracted profiles of surface temperature at the centerplane of the plasma-on side of the airfoil surface under the glaze-icing conditions of $U_\infty = 40$ m/s, $T_\infty = -5°C$, and LWC $= 1.50$ g/m^3.

which can effectively prevent the formation of ice over the airfoil surface during the entire duration of the ice-accretion experiment. Although the same electric voltage was applied to all the DBD plasma actuators, the surface temperatures in the regions near the airfoil leading edge (i.e., near the first DBD plasma actuator) were found to be much lower than those at the downstream locations. It is believed to be closely related to the enhanced convective heat transfer near the airfoil leading edge due to the direct impingement of the supercooled water droplets along with the frozen-cold incoming airflow.

By comparing the surface temperature profiles at different time instances, it can be seen clearly that, with more and more heat added onto the airfoil surface via DBD plasma generation, the surface temperature of the airfoil model was found to increase continuously with the time in general. Although the initial surface temperature in the downstream regions without DBD plasma actuators (i.e., in the downstream regions of $X/D > 0.35$) was found to be below the frozen temperature of water (i.e., as shown in the profile at the time instance of $t = 0.3$ s), their values were to increase rapidly and became above the frozen temperature of water (i.e., $T_w > 0°C$) about 20 s later due to the runback of the warm surface water from the "hot" upstream locations into the cold downstream regions.

Figure 6 shows the variations of the measured surface temperatures as functions of time at three preselected points over the airfoil surface (i.e., the points of A, B, and C as shown in Fig. 6, located at ~5, 25, and 55% chord, respectively), which can be used to reveal the evolution characteristics of the surface temperature over the airfoil/wing model more clearly and quantitatively. As described previously, because the DBD plasma actuators were switched on about 10 s before turning on the water spray system of ISU-IRT, the initial surface temperatures (i.e., the temperature at the time instance of $t = 0$) at point A (i.e., $T_{\#A,t=0} = 2.0°C$) and point B (i.e., $T_{\#B,t=0} = 9.0°C$) were found to be well above the frozen temperature of water (i.e., $T_w > 0°C$), due to the thermal effect induced by DBD plasma generation. The initial surface temperature at point C (i.e., $T_{\#C,t=0} = -2.0°C$) was also found to be slightly higher than the temperature of the incoming airflow (i.e., $T_\infty = -5.0°C$) caused by the convective heat transfer from hot upstream regions.

As shown clearly in Fig. 6, the surface temperature at selected point A was found to decrease rapidly, and it even became negative (i.e., below the frozen temperature of water) at the beginning stage of the ice-accretion experiment (i.e., in the stage of $t < 5$ s). This was caused by the rapid cooling associated with the impingement of the first group of supercooled water droplets onto the airfoil surface near the leading edge. With the continuous heating effect induced by the DBD plasma generation, the surface temperature at point A was found to increase gradually and became greater than the frozen temperature of water

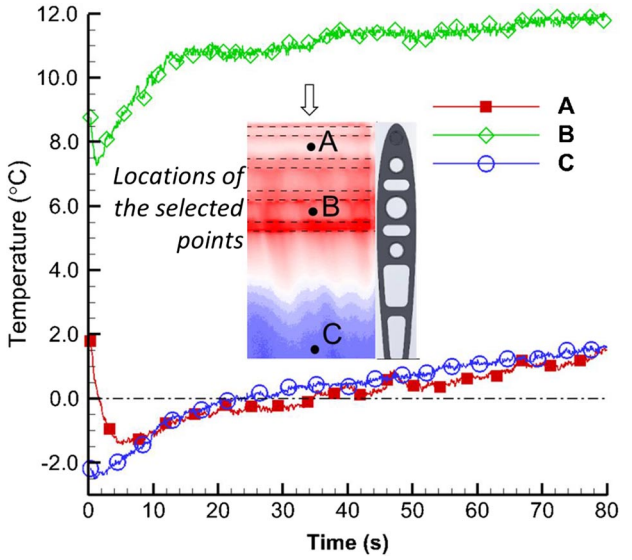

Fig. 6 Time evolutions of the surface temperatures at three preselected points during the ice-accretion experiment with $U_\infty = 40$ m/s, $T_\infty = -5$°C, and LWC = 1.50 g/m^3.

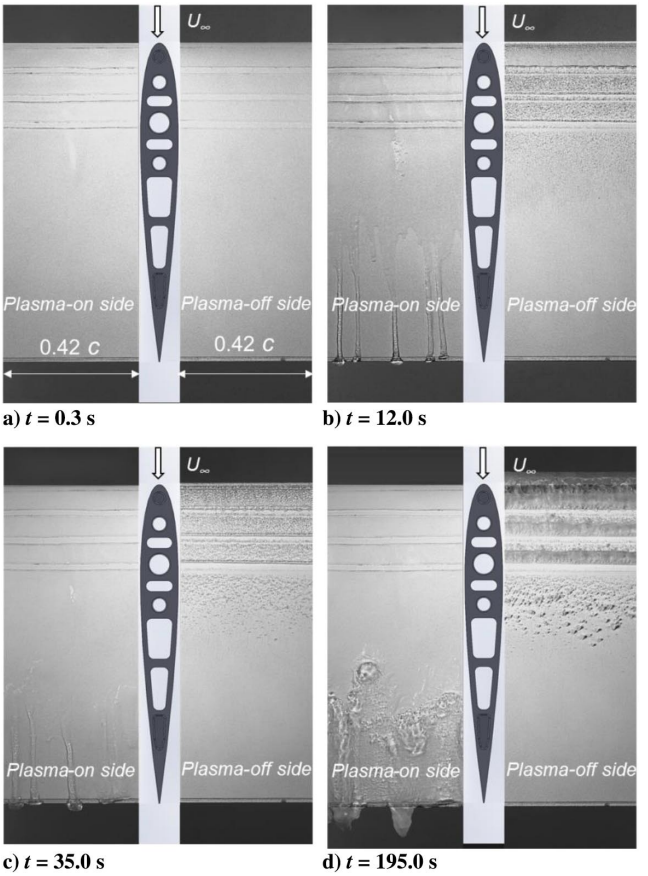

Fig. 7 Typical snapshots of the dynamic ice-accretion process over the airfoil surface under the rime-icing conditions of $U_\infty = 40$ m/s, $T_\infty = -15$°C, and LWC = 1.0 g/m^3.

again at the time instance of $t \approx 35$ s. As time went by, the surface temperature at point A was found to reach a relatively thermal stable state eventually, with the surface temperature being about 2.0°C for the rest of the ice-accretion experiment (i.e., up to $t \approx 300$ s).

As shown schematically in Fig. 6, point B is located at the top of the third plasma actuator (i.e., at ~25% chord). Due to the heating effect induced by the DBD plasma generation from the third plasma actuator and the relatively weaker convective heat transfer at this downstream location, the surface temperature at point B was found to be always much higher than the frozen temperature of water (i.e., $T_{\#B} >> 0$°C). Although the surface temperature at point B decreased slightly at the initial stage of the ice-accretion experiment (i.e., in the stage of $t < 3$ s), the temperature value was found to recover much faster and reach a relatively thermal stable state at about 15 s after starting the ice-accretion experiment. After reaching a relatively thermal stable state, the surface temperature at point B was found to be maintained at ~11.0°C for the rest of the ice-accretion experiment (i.e., up to $t \approx 300$ s) for this test case.

The airfoil/wing model used in the present study was made of polymer-based material, which has very low thermal conductivity. Because the location of point C was away from the DBD plasma actuators, evolution characteristics of the surface temperature at point C were mainly affected by the convective heat transfer process over the airfoil surface. As shown clearly in Fig. 6, due to the heating effect associated with the runback of warm surface water from the hot upstream region, the surface temperatures at point C were found to increase continuously during the ice-accretion experiment. Although the temperature at point C was found to be below the frozen temperature of water initially (i.e., $T_{\#C,t=0} = -2.0$°C), it became greater than the frozen temperature of water quickly (i.e., at $t > 20$ s) due to the heating effect associated with the runback of the warm water. Since $t > 80$ s, the surface temperature at point C was found to be maintained almost constantly at about 2.0°C for the rest of the ice-accretion experiment (i.e., up to $t \approx 300$ s).

C. Effects of Plasma Generation on Ice Accretion Under Rime-Icing conditions

To further explore the anti-/deicing performance of the DBD plasma actuators for aircraft inflight icing mitigation under a typical rime-icing condition, an experimental study was also conducted with the airflow temperature in the ISU-IRT decreased to $T_\infty = -15$°C and LWC = 1.0 g/m^3. Figure 7 shows the typical snapshots to reveal the dynamic ice-accretion process over the airfoil surface under such rime-icing conditions (i.e., $U_\infty = 40$ m/s, $T_\infty = -15$°C, and LWC = 1.0 g/m^3). It is should be noted that the power inputs applied to the DBD plasma actuators were kept at the same levels as those under the glaze-icing condition during the ice-accretion experiment. As revealed clearly in Fig. 7, on the plasma-off side of the airfoil surface, the supercooled water droplets were found to ice up immediately as they impinged onto the airfoil surface due to the much colder temperature for this test case. No obvious rivulet formation or surface water runback were observed during the ice-accretion process, as expected for a typical rime-ice-accretion process. However, on the plasma-on side of the airfoil surface, although no obvious ice accretion could be identified at the front portion of the airfoil surface (i.e., approximately twice the area of the region covered by the DBD plasma actuators), a large chunk of ice was found to accrete eventually over the rear portion of the airfoil surface. This could be explained by the fact that, after impacted onto the warm surface near the airfoil leading edge (i.e., the region protected by the DBD plasma actuators), supercooled water droplets would be heated up and form a thin water film/rivulet flow near the airfoil leading edge, as revealed clearly by Zhang et al. [26]. The unfrozen surface water film would run back, as driven by the boundary-layer airflow over the airfoil surface. Due to the intensive heat transfer between the runback surface water and the boundary-layer airflow over the airfoil surface at a frozen-cold temperature of −15°C, the surface water was found to be frozen gradually as it ran back. As a result, ice accretion was found to take place in the downstream region beyond the area protected by the DBD plasma actuators. As time went by, with the continuous impinging of the supercooled water droplets onto the airfoil surface, more and more surface water mass would be collected and eventually frozen into ice over the rear portion of the airfoil/wing model, i.e., in the downstream region beyond the area protected by the DBD plasma actuators, which was revealed clearly in Fig. 7.

In summary, although the thermal effects induced by the DBD plasma generation were demonstrated to be effective in preventing ice formation and accretion over the protected area under the rime-icing condition with a much colder ambient temperature, the runback

surface water was found to be refrozen gradually in the downstream region beyond the protected area. This is a rather common problem faced by all the thermal-based anti-/deicing systems. A hybrid anti-/deicing concept by integrating DBD plasma heating near the airfoil leading edge with hydro-/ice-phobic coatings [27] over the airfoil surface may offer a promising solution to this problem, which will be explored in the near future. For the hybrid anti-/deicing system, although DBD plasma actuators will be used to cover the region near the airfoil leading edge, the rest of the airfoil surface will be coated with promising hydro-/ice-phobic materials. Although minimized power inputs were applied to the DBD plasma actuators to effectively delaminate the ice accretion near the airfoil leading edge, runback surface water would be easily removed from the hydro-/ice-phobic airfoil surface by aerodynamic shear forces. Such a hybrid anti-/deicing strategy is expected to be able to delay/reject ice accretion over the entire airfoil surface at a much lower power cost than the method with massive brute-force heating over the entire airfoil surface.

IV. Conclusions

An explorative study was conducted to evaluate the effectiveness of leveraging thermal effect induced by dielectric-barrier-discharge (DBD) plasma generation for aircraft icing mitigation. The experimental study was performed in an icing research tunnel available at the Aerospace Engineering Department of Iowa State University. A NACA 0012 airfoil/wing model embedded with two sets of DBD plasma actuators over the airfoil surface was mounted inside the ISU-IRT under typical glaze-/rime-icing conditions pertinent to aircraft inflight icing phenomena. During the experiments, while a high-speed imaging system was used to record the dynamic ice-accretion and transient surface water transport processes over the airfoil surface, an infrared thermal imaging system was also used to map the corresponding surface temperature distributions over the airfoil surface. Based on the side-by-side comparisons of the measurement results (i.e., snapshots of the visualization images and quantitative surface temperature distributions) for the plasma-on case against those of the plasma-off case under the same icing conditions, the effectiveness of using the thermal effects induced by DBD plasma generation for aircraft icing mitigation was evaluated in detail.

It was found that, upon the impingement of supercooled water droplets carried by the incoming airflow onto the airfoil surface, ice accretion would take place immediately over the airfoil surface if the embedded DBD plasma actuators were switched off, as expected. As time went by, with more and more supercooled water droplets impinged onto the airfoil surface, the ice layers accumulated over the airfoil surface were found to become thicker and thicker for the plasma-off case. However, if the plasma actuators were turned on under a typical glaze-ice condition (i.e., $U_\infty = 40$ m/s, $T_\infty = -5$°C, and LWC $= 1.5$ g/m^3), the surface temperatures of the entire airfoil model were found to stay above the water frozen temperature (i.e., $Tw > 0$°C). Due to the thermal effects induced by DBD plasma generation, the supercooled water droplets were found to be heated up, and they formed a layer of warm water film over the airfoil surface instead of being frozen into solid ice. Driven by the boundary-layer airflow over the airfoil surface, the warm liquid water accumulated over the airflow surface was found to run back to further downstream regions, and it shed eventually from the airfoil trailing edge. As a result, the airfoil surface under the typical glaze-ice condition was found to be completely free of ice during the entire ice-accretion experiment.

As for a typical rime-icing case (i.e., under the test conditions of $U_\infty = 40$ m/s, $T_\infty = -15$°C, and LWC $= 1.0$ g/m^3), although the thermal effects induced by the DBD plasma generation were demonstrated to be effective in preventing ice formation and accretion over the area protected by the DBD plasma actuators, the runback surface water was found to be refrozen gradually in the downstream region beyond the protected area due to at the much colder ambient temperature. This is a rather common problem faced by all the thermal based anti-/deicing systems. A hybrid anti-/deicing concept by integrating DBD plasma heating near the airfoil leading edge with hydrophobic/ice-phobic coatings over the airfoil surface was proposed to address this problem, which will be explored in the near future.

It should be noted that, although the present study demonstrated clearly that DBD plasma actuators can be used as a promising anti-/deicing tool for aircraft icing mitigation by taking advantage of the thermal effects associated with DBD plasma generation, a side-by-side comparative study is planned to evaluate the effectiveness of the plasma-based anti-/deicing strategy (i.e., in the term of the required power consumption for anti-/deicing operation) against that of conventional electrothermal heating methods for aircraft icing mitigation under different icing conditions. More comprehensive studies will also be conducted to elucidate the underlying mechanism pertinent to plasma-based anti-/deicing technology in order to explore/optimize design paradigms for the development of effective and robust anti-/deicing strategies to ensure safer and more efficient operation of aircraft in cold weather.

Acknowledgments

The research work is partially supported by Iowa Space Grant Consortium Base Program for Aircraft Icing Studies, with Richard Wlezien as the Director. The authors also gratefully acknowledge the support of the National Science Foundation under award numbers CBET-1064196 and CBET-1435590. The technical assistance of Feng Liu of the University of California, Irvine; Jinsheng Cai of Northwestern Polytechnic University; and Cem Kolbakir of Iowa State University is greatly appreciated.

References

[1] Petty, K. R., and Floyd, C. D. J., "A Statistical Review of Aviation Airframe Icing Accidents in the US," *Proceedings of the 11th Conference on Aviation, Range, and Aerospace*, Sec. 11, No. 2, National Transportation Safety Board, Hyannis, MA, Oct. 2004, https://ams.confex.com/ams/11aram22sls/techprogram/paper_81425.htm [retrieved 20 Oct. 2017].

[2] Gent, R. W., Dart, N. P., and Cansdale, J. T., "Aircraft Icing," *Philosophical Transactions of the Royal Society of London, A: Mathematical, Physical and Engineering Sciences*, Vol. 358, No. 1776, 2000, pp. 2873–2911. doi:10.1098/rsta.2000.0689

[3] Liu, Y., Chen, W. L., Bond, L. J., and Hu, H., "An Experimental Study on the Characteristics of Wind-Driven Surface Water Film Flows by Using a Multi-Transducer Ultrasonic Pulse-Echo Technique," *Physics of Fluids*, Vol. 29, No. 1, 2017, Paper 012102. doi:10.1063/1.4973398

[4] Bragg, M. B., Broeren, A. P., and Blumenthal, L. A., "Iced-Airfoil Aerodynamics," *Progress in Aerospace Sciences*, Vol. 41, No. 5, 2005, pp. 323–362. doi:10.1016/j.paerosci.2005.07.001

[5] Cebeci, T., and Kafyeke, F., "Aircraft Icing," *Annual Review of Fluid Mechanics*, Vol. 35, No. 1, 2003, pp. 11–21. doi:10.1146/annurev.fluid.35.101101.161217

[6] Liu, Y., Waldman, R. M., and Hu, H., "An Experimental Investigation on the Unsteady Heat Transfer Process over an Ice Accreting NACA 0012 Airfoil," *53rd AIAA Aerospace Sciences Meeting*, AIAA Paper 2015-0035, 2015. doi:10.2514/6.2015-0035

[7] Waldman, R. M., and Hu, H., "High-Speed Imaging to Quantify Transient Ice Accretion Process over an Airfoil," *Journal of Aircraft*, Vol. 53, No. 2, 2016, pp. 369–377. doi:10.2514/1.C033367

[8] Fortin, G., Laforte, J. L., and Ilinca, A., "Heat and Mass Transfer During Ice Accretion on Aircraft Wings with an Improved Roughness Model," *International Journal of Thermal Sciences*, Vol. 45, No. 6, 2006, pp. 595–606. doi:10.1016/j.ijthermalsci.2005.07.006

[9] Rutherford, R. B., "De-Ice and Anti-Ice System and Method for Aircraft Surfaces," U.S. Patent No. 6194685 B1, 2001.

[10] Thomas, S. K., Cassoni, R. P., and MacArthur, C. D., "Aircraft Anti-Icing and De-Icing Techniques and Modeling," *Journal of Aircraft*, Vol. 33, No. 5, 1996, pp. 841–854. doi:10.2514/3.47027

[11] Pellissier, M. P. C., Habashi, W. G., and Pueyo, A., "Optimization via FENSAP-ICE of Aircraft Hot-Air Anti-Icing Systems," *Journal of Aircraft*, Vol. 48, No. 1, 2011, pp. 265–276. doi:10.2514/1.C031095

[12] Liu, Y., Bond, L. J., and Hu, H., "Ultrasonic-Attenuation-Based Technique for Ice Characterization Pertinent to Aircraft Icing Phenomena," *AIAA Journal*, Vol. 55, No. 5, 2017, pp. 1602–1609. doi:10.2514/1.J055500

[13] Palacios, J., Smith, E., Rose, J., and Royer, R., "Instantaneous De-Icing of Freezer Ice via Ultrasonic Actuation," *AIAA Journal*, Vol. 49, No. 6, 2011, pp. 1158–1167. doi:10.2514/1.J050143

[14] Kent, R., and Andersen, D., "Canadian Water Quality Guidelines for Glycols—An Ecotoxicological Review of Glycols and Associated Aircraft Anti-Icing and Deicing Fluids," *Environmental Toxicology*, Vol. 14, No. 5, 1999, pp. 481–522. doi:10.1002/(ISSN)1522-7278

[15] Cancilla, D. A., Holtkamp, A., Matassa, L., and Fang, X., "Isolation and Characterization of Microtox®-Active Components from Aircraft De-Icing/Anti-Icing Fluids," *Environmental Toxicology and Chemistry*, Vol. 16, No. 3, 1997, pp. 430–434. doi:10.1002/etc.5620160306

[16] Corke, T. C., Enloe, C. L., and Wilkinson, S. P., "Dielectric Barrier Discharge Plasma Actuators for Flow Control," *Annual Review of Fluid Mechanics*, Vol. 42, No. 1, 2010, pp. 505–529. doi:10.1146/annurev-fluid-121108-145550

[17] Little, J., Takashima, K., Nishihara, M., Adamovich, I., and Samimy, M., "Separation Control with Nanosecond-Pulse-Driven Dielectric Barrier Discharge Plasma Actuators," *AIAA Journal*, Vol. 50, No. 2, 2012, pp. 350–365. doi:10.2514/1.J051114

[18] Enloe, C. L., McLaughlin, T. E., Van Dyken, R. D., Kachner, K. D., Jumper, E. J., and Corke, T. C., "Mechanisms and Responses of a Single Dielectric Barrier Plasma Actuator: Plasma Morphology," *AIAA Journal*, Vol. 42, No. 3, 2004, pp. 589–594. doi:10.2514/1.2305

[19] Kozlov, A. V., and Thomas, F. O., "Plasma Flow Control of Cylinders in a Tandem Configuration," *AIAA Journal*, Vol. 49, No. 10, 2011, pp. 2183–2193. doi:10.2514/1.J050976

[20] Thomas, F. O., Corke, T. C., Iqbal, M., Kozlov, A., and Schatzman, D., "Optimization of Dielectric Barrier Discharge Plasma Actuators for Active Aerodynamic Flow Control," *AIAA Journal*, Vol. 47, No. 9, 2009, pp. 2169–2178. doi:10.2514/1.41588

[21] Wang, J. J., Choi, K. S., Feng, L. H., Jukes, T. N., and Whalley, R. D., "Recent Developments in DBD Plasma Flow Control," *Progress in Aerospace Sciences*, Vol. 62, Oct. 2013, pp. 52–78. doi:10.1016/j.paerosci.2013.05.003

[22] Joussot, R., Boucinha, V., Weber-Rozenbaum, R., Rabat, H., Leroy-Chesneau, A., and Hong, D., "Thermal Characterization of a DBD Plasma Actuator: Dielectric Temperature Measurements Using Infrared Thermography," *40th Fluid Dynamics Conference and Exhibit*, AIAA Paper 2010-5102, 2010. doi:10.2514/6.2010-5102

[23] Van den Broecke, J., "Efficiency and De-Icing Capability of Nanosecond Pulsed Dielectric Barrier Discharge Plasma Actuators," M.S. Thesis, Delft Univ. of Technology, Delft, The Netherlands, 2016.

[24] Meng, X., Cai, J., Tian, Y., Han, X., Zhang, D., and Hu, H., "Experimental Study of Deicing and Anti-Icing on a Cylinder by DBD Plasma Actuation," *47th AIAA Plasmadynamics Lasers Conference*, AIAA Paper 2016-4019, 2016. doi:10.2514/6.2016-4019

[25] Dong, B., Bauchire, J. M., Pouvesle, J. M., Magnier, P., and Hong, D., "Experimental Study of a DBD Surface Discharge for the Active Control of Subsonic Airflow," *Journal of Physics D: Applied Physics*, Vol. 41, No. 15, 2008, Paper 155201. doi:10.1088/0022-3727/41/15/155201

[26] Zhang, K., Wei, T., and Hu, H., "An Experimental Investigation on the Surface Water Transport Process over an Airfoil by Using a Digital Image Projection Technique," *Experiments in Fluids*, Vol. 56, No. 9, 2015, pp. 173. doi:10.1007/s00348-015-2046-z

[27] Waldman, R. M., Li, H., and Hu, H., "An Experimental Investigation on the Effects of Surface Wettability on Water Runback and Ice Accretion over an Airfoil Surface," *8th AIAA Atmospheric and Space Environments Conference*, AIAA Paper 2016-3139, 2016.

C. Wen
Associate Editor